Quantitative Site-specific Reactivity Profiling of S-nitrosylation in Mouse Skeletal Muscle Using Cysteinyl Peptide Enrichment Coupled with Mass Spectrometry.

ARTICLE *in* FREE RADICAL BIOLOGY AND MEDICINE · DECEMBER 2012

Impact Factor: 5.74 · DOI: 10.1016/j.freeradbiomed.2012.12.010 · Source: PubMed

Free Radical Biology and Medicine 57 (2013) 68–78

Contents lists available at SciVerse ScienceDirect

Free Radical Biology and Medicine

journal homepage: www.elsevier.com/locate/freeradbiomed

Original Contributions

Quantitative site-specific reactivity profiling of S-nitrosylation in mouse skeletal muscle using cysteinyl peptide enrichment coupled with mass spectrometry

Dian Su [a], Anil K. Shukla [a], Baowei Chen [a], Jong-Seo Kim [a], Ernesto Nakayasu [a], Yi Qu [a], Uma Aryal [a], Karl Weitz [a], Therese R.W. Clauss [a], Matthew E. Monroe [a], David G. Camp II [a], Diana J. Bigelow [a], Richard D. Smith [a], Rohit N. Kulkarni [b], Wei-Jun Qian [a,*]

[a] Biological Sciences Division, Pacific Northwest National Laboratory, Richland, WA 99352, USA
[b] Joslin Diabetes Center, Harvard Medical School, Boston, MA 02215, USA

ARTICLE INFO

Article history:
Received 17 July 2012
Received in revised form
12 November 2012
Accepted 13 December 2012
Available online 28 December 2012

Keywords:
S-nitrosylation
Redox regulation
Chemical enrichment
Mouse muscle
Proteomics
LC–MS/MS
Free radicals

ABSTRACT

S-nitrosylation, the formation of *S*-nitrosothiol (SNO), is an important reversible thiol oxidation event that has been increasingly recognized for its role in cell signaling. Although many proteins susceptible to S-nitrosylation have been reported, site-specific identification of physiologically relevant SNO modifications remains an analytical challenge because of the low abundance and labile nature of this modification. Herein we present further improvement and optimization of the recently reported resin-assisted cysteinyl peptide enrichment protocol for SNO identification and its application to mouse skeletal muscle to identify specific cysteine sites sensitive to S-nitrosylation by a quantitative reactivity profiling strategy. Our results indicate that the protein- and peptide-level enrichment protocols provide comparable specificity and coverage of SNO-peptide identifications. S-nitrosylation reactivity profiling was performed by quantitatively comparing the site-specific SNO modification levels in samples treated with *S*-nitrosoglutathione, an NO donor, at two different concentrations (i.e., 10 and 100 μM). The reactivity profiling experiments led to the identification of 488 SNO-modified sites from 197 proteins with specificity of ~95% at the unique peptide level, i.e., ~95% of enriched peptides contain cysteine residues as the originally SNO-modified sites. Among these sites, 281 from 145 proteins were considered more sensitive to S-nitrosylation based on the ratios of observed SNO levels between the two treatments. These SNO-sensitive sites are more likely to be physiologically relevant. Many of the SNO-sensitive proteins are localized in mitochondria, contractile fiber, and actin cytoskeleton, suggesting the susceptibility of these subcellular compartments to redox regulation. Moreover, these observed SNO-sensitive proteins are primarily involved in metabolic pathways, including the tricarboxylic acid cycle, glycolysis/gluconeogenesis, glutathione metabolism, and fatty acid metabolism, suggesting the importance of redox regulation in muscle metabolism and insulin action.

Reversible oxidative modifications on protein thiols have been recognized as important and ubiquitous posttranslational modifications that are essential for redox signaling and regulation in normal physiological and pathological processes [1–4]. In particular, several forms of reversible oxidation of cysteine thiols, including S-nitrosylation, S-glutathionylation, and S-sulfenic acid, have been increasingly emphasized for their roles in integrating both reactive oxygen and reactive nitrogen species (ROS/RNS)[1] to mediate cellular signaling pathways [1,5,6].

Among these reversible forms of thiol oxidation, S-nitrosylation, the coupling of a nitric oxide (NO) moiety to a reactive cysteine thiol to form an *S*-nitrosothiol (SNO), has received considerable interest as a redox-based signaling mechanism [7–21]. S-nitrosylation is primarily formed by NO that is generated by nitric oxide synthases or various SNO-containing small molecules (e.g., *S*-nitrosoglutathione, GSNO) that serve as NO donors [11]. Much like phosphorylation, S-nitrosylation plays an important role in modulating a broad spectrum of cellular signaling pathways by regulating enzyme activities and protein–protein interactions. For example, S-nitrosylation has been reported to play a central role in cell apoptosis through the reversible inhibition of caspase-3 [22]. The precise coordination between S-nitrosylation and denitrosylation by denitrosylases

Abbreviations: ROS/RNS, reactive oxygen and reactive nitrogen species; SNO, *S*-nitrosothiol; GSNO, *S*-nitrosoglutathione; NEM, *N*-ethylmaleimide

* Corresponding author. Fax: +1 509 371 6564.
E-mail addresses: Weijun.qian@pnnl.gov, weijunqian7@gmail.com (W.-J. Qian).

0891-5849/$ - see front matter © 2012 Elsevier Inc. All rights reserved.
http://dx.doi.org/10.1016/j.freeradbiomed.2012.12.010

contributes to the regulation of cellular SNO signaling [23–25]. The dysregulation of S-nitrosylation has been implicated in many pathologies, including metabolic diseases, neurodegenerative diseases, and cancer [17]. Therefore, elucidation of the specific targets and dynamic regulation of S-nitrosylation is of interest to gain better mechanistic understanding of cellular signaling and disease pathogenesis and for developing novel therapeutic strategies.

In this study, we aimed to identify specific proteins and cysteine sites that are sensitive to S-nitrosylation in mouse skeletal muscle by applying the concept of quantitative reactivity profiling [26]. Skeletal muscle is a major tissue in which ROS/RNS are known to play an important role in regulating muscle metabolism and cellular functions under both normal and pathological conditions [27,28]. A number of studies have reported the significance of S-nitrosylation on specific proteins for regulating muscle cellular functions and insulin resistance, including the calcium release channel ryanodine receptor and several key insulin-signaling proteins [29–31]; however, few studies have identified specific SNO sites in muscle on a broad scale [32,33] because of the challenges associated with site-specific detection of SNO modifications.

A number of methodologies have been reported for the detection of SNO-modified proteins [34], with the most common concept centered on the conversion of the SNO group back to a free thiol group for selective enrichment. This concept was first introduced as the biotin-switch technique (BST) by Jaffrey et al. in 2001 [35–37]. When coupled with mass spectrometry (MS), the BST has been extended for site identification and quantification of SNO modification [38–41]. More recently, a resin-assisted capture strategy was reported for LC–MS/MS-based SNO identification [42,43], in which a cysteinyl peptide enrichment approach, initially developed by our group [44] using Thiopropyl Sepharose 6B resin, was adapted to address the nonspecificity issue in the previous avidin–biotin-based enrichment method [42]. Here, we further assessed and optimized the resin-assisted capture approach and introduced the use of on-resin isobaric labeling for quantitative reactivity profiling of S-nitrosylation in muscle treated with GSNO as the NO donor. The endogenous concentration of SNOs, such as GSNO, was reported to be in the low micromolar range. For example, the level of SNOs was reported to be 0.5–10 μM in human airways [45], and the tissue concentration of GSNO was estimated to be 6–8 μM in rat cerebellum [46]. Herein, we utilized two doses of GSNO treatment, with one dose (10 μM) close to physiological levels and the other (100 μM) higher to profile the reactivity of individual protein cysteine sites to
S-nitrosylation. A total of 488 SNO-modified cysteine sites from 197 proteins were identified from mouse muscle, with different levels of sensitivity being quantified based on the ratios of observed SNO levels between the two treatments.

Materials and methods

Chemicals

BCA protein assay reagents, silver stain kit, and spin columns were purchased from Thermo Fisher Scientific (Rockford, IL, USA). Sequencing grade-modified porcine trypsin was from Promega (Madison, WI, USA). iTRAQ (isobaric tags for relative and absolute quantitation) reagents were from AB SCIEX (Foster City, CA, USA). The SeeBlue Plus2 protein standard was from Invitrogen (Carlsbad, CA, USA). Thiopropyl Sepharose 6B affinity resin was from Amersham Biosciences (Uppsala, Sweden). Tris/glycine/sodium dodecyl sulfate (SDS) buffer, Laemmli sample loading buffer, and Tris–HCl precast gel with 4–20% linear gradient were all from Bio-Rad Laboratories (Hercules, CA, USA). Unless otherwise noted, all other chemicals and reagents were purchased from Sigma–Aldrich (St. Louis, MO, USA).

Mouse skeletal muscle samples

The quadriceps femoris muscle was isolated from 6-month-old male C57BL6J mice fed a standard chow diet. The frozen tissue was homogenized in buffer with 50 mM NaCl, 50 mM NH_4HCO_3 (pH 7.8), using a Silverson L4R homogenizer. The homogenate was centrifuged for 20 min at 500*g* at 4 °C, and the supernatant was filtered through two layers of cheesecloth. The filtrate was further centrifuged for 10 min at 5000*g* at 4 °C, and the protein concentration of the supernatant was measured using a BCA assay. Supernatants were stored at −80 °C until further use.

Induction of S-nitrosylation in muscle samples

To induce S-nitrosylation, the muscle homogenates reconstituted in buffer 1 (250 mM HEPES, pH 7.7, 1 mM EDTA, 0.1 mM neocuproine) were treated with either 10 or 100 μM GSNO from a stock solution in dimethyl sulfoxide (DMSO). For control, the samples were treated with 1% (v/v) DMSO. The final samples containing 500 μg proteins per sample with each in a 1-ml volume were incubated in a Thermomixer (Fisher Scientific, Pittsburgh, PA, USA) in the dark at 37 °C for 30 min. To induce S-nitrosylation in a mixture of bovine serum albumin (BSA) and glyceraldehyde-3-phosphate dehydrogenase (GAPDH), a 1-ml volume of the final sample solution containing 10 μM BSA, 5 μM GAPDH, and 1% DMSO with (treated) or without (untreated) 100 μM GSNO was incubated for 30 min at 37 °C.

Excess GSNO was removed in the dark with 4 ml Amicon Ultra 30K molecular-weight cutoff (MWCO) filter units (EMD Millipore, Billerica, MA, USA) by adopting the filtered-assisted sample preparation (FASP) protocol [47]. Briefly, the samples were transferred quickly to the filters containing 3 ml of cold water and centrifuged at 4000*g* for 15–30 min at 4 °C. The procedure was repeated three times. Samples were concentrated to ~100 μl.

Alkylation of free cysteines

After the samples were concentrated, 100 μl of 20% SDS and 800 μl (4 volumes of the sample) of 20 mM *N*-ethylmaleimide (NEM) in buffer 1 were added to the Amicon filters. Samples were alkylated by incubating in a Thermomixer in the dark at 55 °C and shaking for 30 min. After alkylation, excess NEM reagents were removed by buffer exchange with 8 M urea three times and Milli-Q water once by centrifugation at 4000*g* for 30 min at 4 °C. A 1-μl aliquot of 20% SDS was added to the final concentrated sample solutions (~50 μl), and the samples were then transferred to microcentrifuge tubes. Buffer 2 (250 mM HEPES, pH 7.7) was then added to adjust the solution to a final volume of ~130 μl. Samples were then centrifuged at 10,000*g* for 2 min to remove any undissolved debris. The protein concentration in the supernatant of each sample was measured by the BCA assay. Same amounts of protein samples (~60 μl) were used for protein- and peptide-level enrichment after dilution to 120 μl with buffer 2.

Protein- and peptide-level enrichment of free thiols after the reduction of SNO

Sodium ascorbate (NaASC) and CuCl stock solutions were added to all samples to reach final concentrations of 5 mM NaASC and 5 μM CuCl to selectively convert SNO back to free thiol. One exception was the pre-ASC condition, a negative control, in which

sample was treated with NaASC/CuCl instead of GSNO before alkylation with NEM.

For protein-level enrichment, the samples were immediately transferred to Handee minispin columns with 35 mg prewet and prewashed Thiopropyl Sepharose 6B resin and 25 mM HEPES buffer as described previously [48,49]. Enrichment of free cysteine-containing proteins was carried out by incubating the samples in a Thermomixer at room temperature with shaking at 850 rpm for 2 h. Nonspecifically bound proteins were removed by washing five times with the following solutions: (1) 8 M urea, (2) 2 M NaCl, (3) 80% acetonitrile (ACN) with 0.1% trifluoroacetic acid (TFA), and (4) 25 mM HEPES (pH 7.7). To perform the on-resin digestion, a premixed 120 μl solution containing 25 mM HEPES buffer (pH 7.7), 0.1% SDS, 8.8 μg trypsin, and 1 mM $CaCl_2$ were added to the columns and the samples were incubated at 37 °C with shaking at 850 rpm for 3 h. Nonspecifically bound peptides were washed away using the same procedure as described above for removing nonspecifically bound proteins.

For peptide-level enrichment, in-solution protein digestion for each sample was carried out in the dark at 37 °C for 3 h by adding 8.8 μg trypsin and 1 mM $CaCl_2$ to each sample. After digestion, 5 mM NaASC and 5 μM CuCl were added to reduce SNO groups to free thiols. The samples were immediately transferred to the spin columns with 35 mg prewet and prewashed Sepharose 6B resin as described above. Cysteinyl peptide enrichment was carried out by incubating the samples on a Thermomixer at room temperature with shaking at 850 rpm for 2 h. Nonspecifically bound peptides were washed applying the same procedure as described above.

On-resin iTRAQ labeling

On-resin isobaric labeling using four-plex iTRAQ reagents was then performed for both peptide- and protein-level enrichments to achieve relative quantification. Ethanol (140 μl) was added to the manufacturer-provided iTRAQ reagents to dissolve/dilute them. Then, 30 μl of dissolution buffer and 75 μl of the above iTRAQ reagent solutions were added to the spin columns. The labeling reaction was carried out at room temperature with shaking at 850 rpm on a Thermomixer for 1 h. The reaction was stopped by adding 8 μl of 5% $NH_2OH \cdot HCl$ in 200 mM triethylammonium bicarbonate buffer followed by incubation at room temperature with shaking at 850 rpm for 15 min. The excess iTRAQ reagents were removed by washing five times with the following solutions: (1) 80% ACN/0.1% TFA and (2) 25 mM ammonium bicarbonate (pH 7.8).

Cys-peptides were eluted by incubation with 20 mM dithiothreitol (DTT) in 100 μl of 25 mM ammonium bicarbonate for 30 min followed by rinsing with 100 μl of 80% ACN/0.1% TFA. Cys-peptide samples were then concentrated in a Thermo Scientific Savant SpeedVac concentrator and adjusted to a final volume of 30 μl with water. The final Cys-peptide sample contained ~200 mM DTT, which prevented free thiols from oxidation before LC–MS/MS analysis. Equal amounts of the samples from each iTRAQ labeling channel were then mixed to generate the final sample for LC–MS/MS analyses.

SDS–polyacrylamide gel electrophoresis (PAGE)

SDS–PAGE was carried out with a 4–20% precast linear gradient Tris–HCl polyacrylamide gel (Bio-Rad) to assess enrichment efficiency and total SNO levels. Equal volumes (5 μl) of the above Cys-peptide sample and Laemmli sample buffer (Bio-Rad) were mixed and then incubated at 95 °C for 5 min. Meanwhile, 1 μl of SeeBlue Plus2 protein standard was directly loaded onto the gel. Gel electrophoresis was run at 170 V for 25 min in Tris/glycine/SDS buffer (Bio-Rad). After electrophoresis, the gel image was developed with silver staining following the manufacturer's standard protocol.

Saville assay for measuring SNO levels

The Saville assay was performed to measure the SNO concentration in various samples. Efficiency at inducing S-nitrosylation and reduction steps was evaluated by measuring the SNO concentrations before and after induction and reduction, respectively. Twofold serial dilutions of GSNO ranging from 25 to 1.56 μM were used to generate the standard curves. A standard protocol reported previously was followed to measure the SNO signals at 540 nm [50]. Briefly, 50 μl each of the nitrosylated samples after GSNO removal was incubated with 50 μl of solution A (1% (w/v) sulfanilamide in 0.5 M HCl) or solution B (solution A containing 0.2% (w/v) $HgCl_2$) at room temperature for 5 min in separate wells of a 96-well plate. Samples were then treated with 100 μl solution C (0.02% (w/v) *N*-(1-naphthyl)ethylenediamine dihydrochloride in 0.5 M HCl) and incubated for another 5 min at room temperature. Absorbance was immediately measured at 540 nm using a Molecular Devices (Sunnyvale, CA, USA) SpectraMax Plus reader. The SNO concentrations of samples were determined by the difference in absorbance between the samples treated with solution B and those treated with solution A according to the GSNO standard curves.

LC–MS/MS analyses

All the samples were analyzed by LC–MS/MS with two technical replicates. Typically, 7 μl of each sample was loaded onto a homemade 65-cm-long reversed-phase capillary column with 75-μm inner diameter packed using 3-μm Jupiter C18 particles (Phenomenex, Torrance, CA, USA). The HPLC system consisted of a custom configuration of 100-ml Isco Model 100 DM syringe pumps (Isco, Lincoln, NE, USA), two-position Valco valves (Valco Instruments Co., Houston, TX, USA), and a PAL autosampler (Leap Technologies, Carrboro, NC, USA) that allowed fully automated sample analysis across four separate HPLC columns [51]. The system was operated at a constant pressure of 10,000 psi with an exponential gradient starting with 100% of mobile phase A (0.1% formic acid in water) to 60% of mobile phase B (0.1% formic acid in acetonitrile) over the course of 100 min.

MS analysis was performed on a Thermo Scientific LTQ-Orbitrap Velos mass spectrometer (Thermo Scientific, San Jose, CA, USA) coupled with an electrospray ionization interface using home-made 150-μm o.d. × 20-μm i.d. chemically etched electrospray emitters [52]. Full MS spectra were recorded at a resolution of 100 K (for ions at m/z 400) over the range of m/z 400–2000 with an automated gain control (AGC) value of 1×10^6. MS/MS was performed in the data-dependent mode with an AGC target value of 3×10^4. The six most abundant parent ions were selected for MS/MS using high-energy collisional dissociation with a normalized collision energy setting of 40%. Precursor ion activation was performed with an isolation width of 2 Da, a minimal intensity of 500 counts, and an activation time of 10 ms.

Data analysis

LC–MS/MS raw data were converted into dta files using Extract_MSn (version 3.0) in Bioworks Cluster 3.2 (Thermo Fisher Scientific, Cambridge, MA, USA), and the SEQUEST algorithm [53] (version 27, revision 12) was used to search all MS/MS spectra against the mouse genome sequence database (UniProt, released on 5 May 2010). The key search parameters used were 50 ppm tolerance for precursor ion masses, 0.05 Da for fragment ion masses, a maximum of two missed tryptic cleavages, dynamic

oxidation of methionine (+15.9949 Da), dynamic NEM modification of cysteine (+125.0477 Da), and static iTRAQ modification of lysine and N-termini (+144.1021 Da).

The decoy-database searching methodology [54,55] was used to control the false discovery rate at the unique peptide level to $<1\%$. MS generating-function (MSGF) scores were generated for each identified spectrum by computing rigorous p values (spectral probabilities) [56]. For those with mass measurement error within 5 ppm, fully tryptic peptides with MSGF score $<1\times10^{-8}$ and partially tryptic peptides with MSGF score $<1\times10^{-10}$ were accepted as identifications. For those with mass measurement error >5 ppm, but picked for fragmentation as nonmonoisotopic peaks, only fully tryptic peptides with a MSGF score $<1\times10^{-10}$ were accepted. For quantification purposes, only peptides with reporter ion intensity for the 100 μM GSNO-treated conditions of >200 and a ratio of control/100 μM GSNO ($R_{C/100}$) and/or pre-ASC/100 μM GSNO ($R_{P/100}$) of <0.2, i.e., at least fivefold SNO signal increase in response to GSNO treatment, were considered confident S-nitrosylated peptides. Gene ontology (GO) and KEGG (Kyoto Encyclopedia of Genes and Genomes) pathway analyses were performed using the DAVID functional annotation [57,58]. Cellular component and biological process categorization of the detected proteins were based upon GO terms with relatively broad categories to better represent the data. Protein interaction network analysis was done using Ingenuity pathway analysis (www.ingenuity.com).

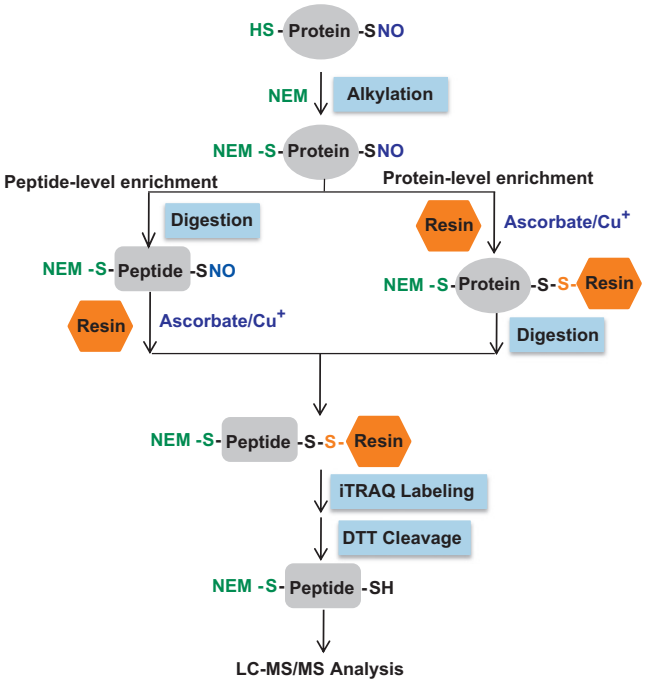

Fig. 1. Schematic workflow of site-specific SNO identification by cysteinyl peptide enrichment and LC–MS/MS analysis. NEM was used to alkylate the free thiols. Ascorbate coupled with CuCl was used for selective reduction of SNO. iTRAQ labeling of enriched Cys-peptides was carried out on-resin, followed by DTT elution. Eluted Cys-peptides were submitted to LC–MS/MS analysis without further cleanup.

Results and discussion

Optimization of the analytical approach

The resin-assisted capture approach for site-specific SNO detection [42], which utilized the cysteinyl-peptide enrichment technique initially developed by our group [48,49], was adapted and modified for enrichment and identification of SNO modification in this work. The overall analytical strategy is illustrated in Fig. 1. Briefly, free thiols are initially blocked by alkylation. Protein samples are either subjected to SNO reduction by ascorbate followed by protein-level enrichment or subjected to proteolytic digestion and SNO reduction followed by enrichment at the peptide level using a Thiopropyl Sepharose 6B resin. The enriched Cys-peptides on the resin were labeled with iTRAQ reagents, which were subsequently released by elution with DTT to facilitate site-specific identification and quantification of the SNO levels by LC–MS/MS.

Because site-specific SNO identification is an indirect detection strategy based on the detection of free cysteine thiols converted from formerly SNO-modified cysteine residues, the potential free thiols from disulfide exchange or breakage represent a potential source of interference and false site identifications [36]. Here, NEM was used as the alkylation agent instead of the methylmethane thiosulfonate used previously, which forms disulfides with free thiols and thus represents a potential source of nonspecific free thiols that may be generated during the digestion and enrichment processes. To minimize sample loss during sample processing, the FASP method [47] was used to remove excess reagents after each reaction step, instead of the commonly used acetone precipitation procedure. The MWCO filter was used as a reaction vessel as well as for removing excess reagents after each reaction. Cys-enrichment was carried out with Thiopropyl Sepharose 6B resin in a spin column [48] with a reaction volume of 100–150 μl to achieve the best efficiency and specificity. A small percentage of SDS (0.1%) was included for both reduction/enrichment and on-resin digestion to obtain a better recovery of enriched peptide samples (Supplementary Fig. 1).

To achieve good detection sensitivity, it is important to ensure effective reduction or denitrosylation in the conversion of SNO to free thiols. At each step in the procedure, the SNO level was assessed with the Saville assay, thus optimizing the conditions for SNO reduction. We used GSNO as the NO donor because it is the main endogenous nonprotein NO source in cells [45]. There has been a controversy as to whether copper should be coupled with ascorbate as a catalyst for the reduction step and whether ascorbate could cause undesired disulfide reduction [37,59–64]. Sinapinic acid has been recently proposed as an alternative reducing agent for SNO [65]. To obtain the optimal reduction condition, reducing agents, including ascorbate with and without copper and sinapinic acid, were assessed for their reduction efficiency using standard BSA protein samples. Without Cu^+, we observed SNO reduction efficiencies of 3, 8, and 16% for buffer only, 1 mM ascorbate, and 10 mM ascorbate, respectively (Supplementary Table 1). With the inclusion of 1 μM Cu^+, ~100% SNO reduction efficiency was observed with 1 mM ascorbate, supporting that Cu^+ is a necessary catalyst for achieving a complete reduction. However, our results showed that sinapinic acid provided a reduction efficiency of only 24% following the reported protocol [65]. Therefore, the combination of ascorbate and Cu^+ was the optimal condition for complete SNO reduction.

On-resin iTRAQ labeling was introduced for quantifying the levels of SNO modifications under different biological conditions in one single experiment [66,67]. The isobaric mass tags covalently attach to amines at the N-terminus and lysine residues. The fragmentation of the mass tags generates corresponding reporter ions whose intensities correspond to the relative abundances of the peptide from different biological samples. The on-resin labeling strategy enables the easy removal of excess iTRAQ reagents for labeling very small amounts of peptide samples. Portions of the enriched Cys-peptide samples released by DTT were subjected to SDS–PAGE for the purpose of quality control (Fig. 2B).

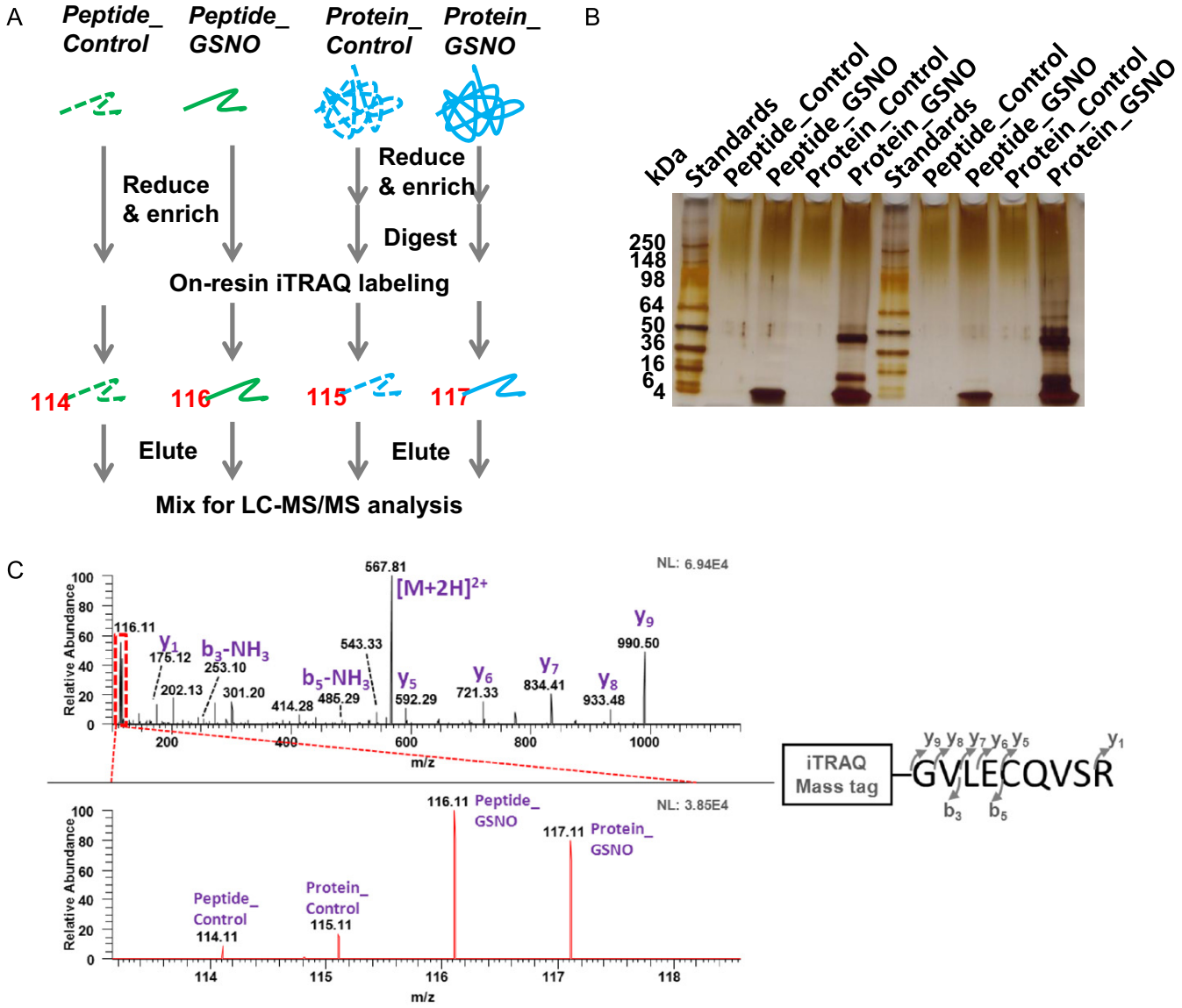

Fig. 2. Experimental strategy for comparing peptide- vs protein-level enrichments. (A) Experimental design applying on-resin iTRAQ-labeling. (B) Silver-staining image of SDS–PAGE of enriched Cys-peptides. For each lane of the 4–20% Tris–HCl precast gel, 5 of 30 µl of DTT-eluted Cys-peptides was loaded. The higher protein bands in protein-level enrichment samples indicate incomplete on-resin digestion. (C) An MS/MS spectrum of the Cys-peptide GVLECQVSR from obscurin protein and its zoom-in spectrum of reporter-ion region showing the SNO abundance increased in response to GSNO treatment.

Comparison of protein- and peptide-level enrichments of SNO-modified peptides

The enrichment of free cysteine-containing peptides (converted from formerly SNO-modified peptides) by Thiopropyl Sepharose 6B resin can be performed either at the peptide level after protein digestion [48] or directly at the protein level followed by tryptic digestion and the removal of nonspecific peptides [42]. However, it was unclear whether one protocol performs better than the other. To compare the performance of protein-level versus peptide-level enrichments for SNO-modified peptides, we utilized control and 100 µM GSNO-treated conditions for enrichment of SNO-peptides in mouse muscle. The same sample amounts were used for peptide- and protein-level enrichments. After enrichment, the four enriched SNO-modified peptides from the four samples (peptide-level control, protein-level control, peptide-level GSNO, and protein-level GSNO conditions) were labeled with the four-plex iTRAQ reagents on-resin for quantification (Fig. 2A). Fig. 2B shows the gel image of final eluted peptides from two independent experiments as processing replicates. Reproducible increases in band intensities of enriched Cys-peptides in response to GSNO treatment for both peptide- and protein-level enriched samples were observed. It is worth noting that we did not observe significant amounts of Cys-peptides in control samples on the gel, indicating that the specificity of enriching formerly SNO-modified peptides was quite high. Although the enrichment performances of peptide-level and protein-level may be comparable, the eluted peptides from protein-level enrichment clearly showed some higher molecular weight bands, indicating that on-resin digestion after enrichment of Cys-proteins was not complete.

The final peptide-enriched samples were further analyzed by LC–MS/MS to compare their performance. Fig. 2C shows an example of MS/MS fragmentation of an identified SNO-modified peptide and the corresponding increases in SNO levels in response to GSNO treatment based on the reporter ion intensities. The

Venn diagram (Fig. 3A) of SNO-modified peptides identified from peptide-level and protein-level enrichment samples showed that the two protocols resulted in a nearly identical set of peptides based on their high overlap. Enrichment specificities are quite similar with 95.3 and 95.0% Cys-containing peptides among all peptides identified for peptide- and protein-level enrichments, respectively. The overall SNO signal level for each sample was calculated by summing the reporter ion intensities for all Cys-containing peptides in each of the iTRAQ channels. Fig. 3B shows the fold increases in overall SNO signal levels by comparing the GSNO-treated conditions against the controls. The observed fold increases in response to GSNO treatments for peptide- and protein-level enriched samples were 20- and 27-fold, respectively, which were not statistically significant based on the data from the two independent experiments. Therefore, protein-level and peptide-level enrichment protocols offer comparable performance. Because of the relative simplicity of the protein-level enrichment protocol, it was used for subsequent quantitative reactivity profiling of S-nitrosylation.

To ensure that high enrichment efficiency at the protein level was achieved, a second enrichment on the flow-through from 500 μg of the 100 μM GSNO-treated sample, which contained

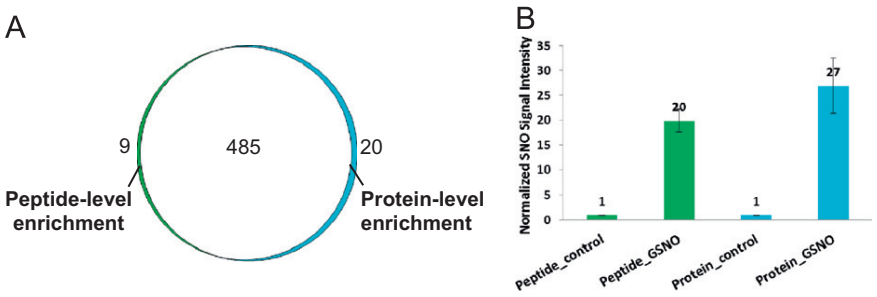

Fig. 3. Comparison of peptide- and protein-level enrichments. (A) Venn diagram of SNO-modified Cys-peptides. The identification numbers are the sums of two independent experiments and their two technical LC–MS replicates. (B) The overall SNO signal increase. The MS/MS reporter ion intensities were calculated from the sums of two independent experiments and their two technical MS replicates for all Cys-peptides and were then normalized against control conditions. Error bars indicate the standard deviation values between two experiments.

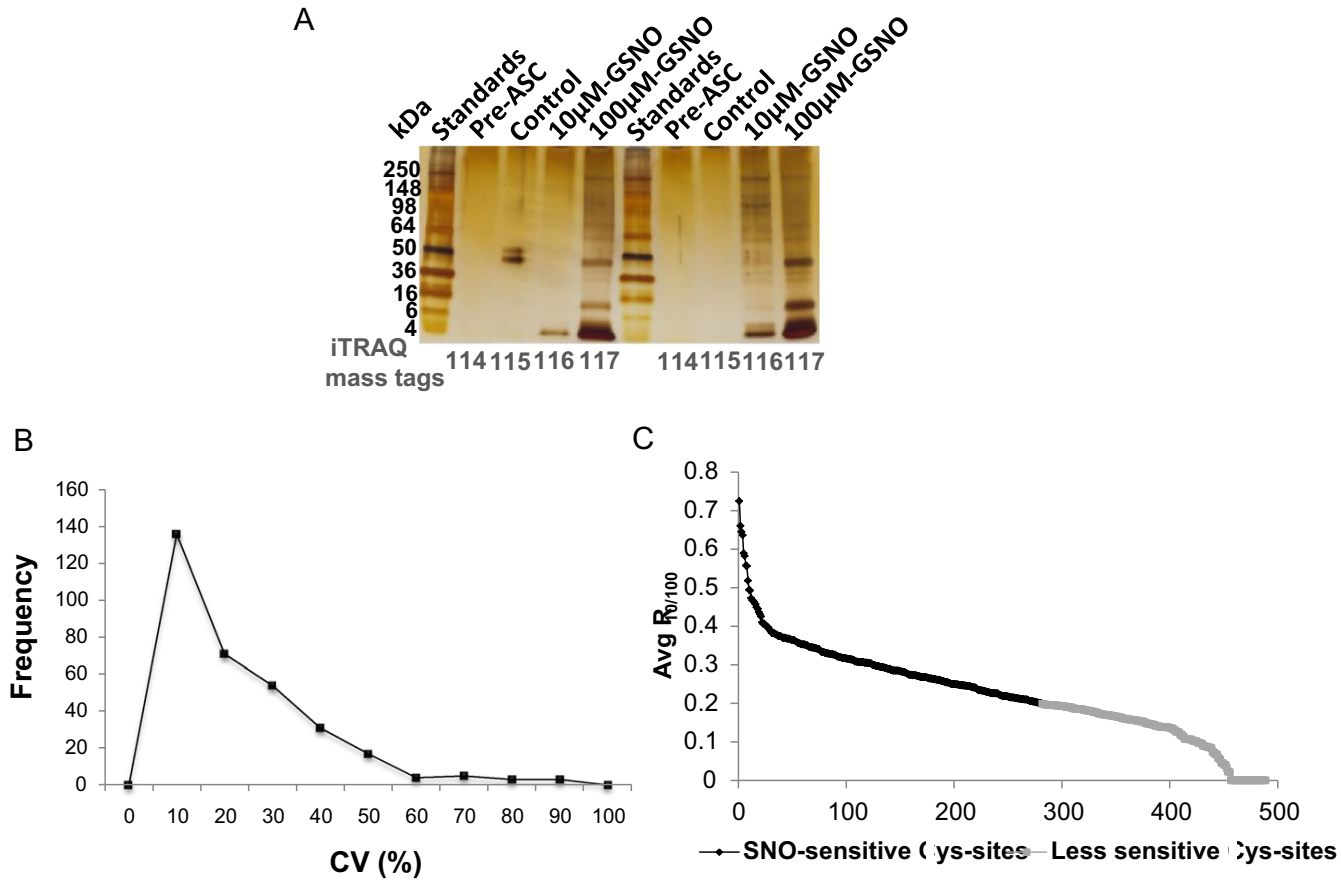

Fig. 4. Assessment of the relative reactivity of Cys sites to S-nitrosylation. (A) Silver-staining image of SDS–PAGE assay of enriched Cys-peptides from two independent experiments. (B) CV distribution of $R_{10/100}$ values of SNO-modified Cys-peptides identified from the two independent experiments. Unique peptides from the two technical MS replicates were combined, and their reporter ion intensities were summed. (C) Relative reactivity of SNO-modified Cys sites detected from the two independent experiments. The *y*-axis values are the average of $R_{10/100}$ values of the two independent experiments. SNO-sensitive Cys sites are depicted in black with average $R_{10/100}$ values >0.2, and less-sensitive Cys sites are in gray.

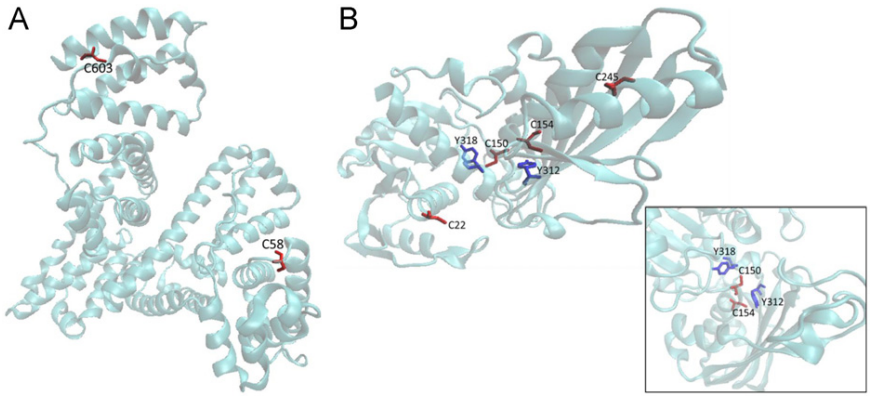

Fig. 5. Illustration of selected Cys sites in protein crystal structures. (A) Crystal structure model of mouse serum albumin, which is built upon the crystal structure of human serum albumin (PDB ID 1N5U). (B) Crystal structure model of GAPDH. Inset is a top view of the enzyme pocket where C150 and C154 are located.

mostly non-Cys-proteins, was performed. The enriched peptides from both enrichments were compared by SDS–PAGE. High enrichment efficiency was confirmed based on the very low gel-band intensity of the second enrichment compared to that from the first enrichment (Supplementary Fig. 2). Similarly, we also performed a double enrichment of total native oxidized Cys-proteins and observed that the resin capability was sufficient to enrich all oxidized proteins from 500 μg of total lysate.

Relative reactivity of Cys sites to S-nitrosylation

Because most studies on S-nitrosylation are based on *in vitro* treatments with NO donors [37], it is unclear whether these detected SNO sites have functional relevance for redox regulation. It has been hypothesized that sites with high reactivity are more likely to be functionally relevant under endogenous conditions [26]. We thus sought to perform quantitative reactivity profiling of S-nitrosylation on Cys sites. It is generally accepted that thiol reactivity involves the nucleophilic attack of the thiolate ion on an electrophile [2]. The reactivity of specific thiols is mainly determined by the accessibility and pK_a of the thiol, which rely on the tertiary structure of proteins and the local microenvironment, respectively [68]. We assessed the reactivity of Cys sites to S-nitrosylation by treating muscle homogenates with two concentrations of GSNO (i.e., 10 and 100 μM) and quantifying the levels of SNO using iTRAQ labeling. Two control samples and two samples treated with 10 and 100 μM GSNO were labeled with four-plex iTRAQ reagents for relative quantification. The reactivity of individual cysteine residues was assessed based on the ratios of observed reporter ion intensities, indicative of the SNO levels, of the low and high GSNO concentrations, i.e., $R_{10/100}$. To assess the reproducibility of such reactivity measurements, we plotted the distribution of coefficient of variation (CV) values of $R_{10/100}$ ratios across the two processing replicates in Fig. 4A (Supplementary Tables 2 and 3). An overall good reproducibility was observed with CV $<30\%$ for the majority of the peptides measured (Fig. 4B).

It was anticipated that low-reactivity Cys sites should show a concentration-dependent increase in SNO levels; i.e., the intensity ratios of SNO-modified peptides between 10 and 100 μM GSNO treatments are close to 0.1 ($R_{10/100} \approx 0.1$) [26], whereas high-reactivity Cys sites should have higher response to low concentration of GSNO, i.e., $R_{10/100} \gg 0.1$. For example, 10 μM GSNO could maximally nitrosylate a given sensitive Cys site to a level close to 100% in terms of stoichiometry. In this case, the $R_{10/100}$ ratio for this sensitive Cys site would be close to 1. To further examine the fraction of sensitive Cys sites, we roughly classified those Cys sites (Supplementary Tables 3 and 4) with $R_{10/100} > 0.2$ as sites relatively sensitive to S-nitrosylation as displayed in Fig. 4C because the observed ratios are at least twice the expected dose response ratio 0.1. In total, 281 Cys sites from 145 proteins were considered sensitive to S-nitrosylation.

These Cys sites with relatively high reactivity to S-nitrosylation were presumably more likely to be functionally relevant or be endogenously nitrosylated for regulating enzyme activities or protein–protein interactions, whereas sites with low reactivity may represent the products of random oxidation. An example was the cysteine-rich protein serum albumin, which contains 36 cysteines with 17 disulfide bonds and 2 free thiols (C58 and C603). We were able to identify C58 as the SNO-sensitive site with an $R_{10/100}$ of ~0.6, but not C603. The Swiss Model crystal structure of mouse serum albumin shows that C58 is located within a solvent-accessible loop region, whereas C603 is buried within the structure on an α-helix (Fig. 5A).

Table 1 shows the relative reactivity of some SNO-sensitive Cys sites from selected proteins. One example was GAPDH, a well-known redox-sensitive protein [69]. In this study, the residues C22, C150, C154, and C245 were identified as SNO sites. GAPDH has a central function in glycolysis by catalyzing the reversible oxidative phosphorylation of glyceraldehyde 3-phosphate to 1,3-bisphosphoglycerate in the presence of nicotinamide adenine dinucleotide and inorganic phosphate. GAPDH was also reported to exert several functions, such as cell apoptosis, and has been shown to undergo S-nitrosylation in the nucleus, an event critical for NO-induced cell death [70]. Although it was reported that C150 is the potential active site of this enzyme and the site susceptible to S-nitrosylation or oxidation [71], our work confidently identified that both C150 and C154 are sensitive to S-nitrosylation. Disulfide bond formation was also reported between C150 and C154 [72]. Although C150 is reported as the active site of the enzyme, detection of C154 in the vicinity can be attributed to the similar local redox environment according to the Swiss Model crystal structure based on human GAPDH (PDB ID 1U8F). Both C150 and C154 are close to a tyrosine residue, namely Y318 (3.18 Å) and Y312 (3.37 Å), respectively (Fig. 5B). In addition, C22 and C245 were also identified as sensitive to S-nitrosylation. C22 is located near the adjoining part of α-helix and loop regions and thus is easily accessible to the NO donor. However, C245 is located on a β-sheet (Fig. 5B). It is worth noting that C150, C154, and C245 were also identified as SNO-modified sites in previous studies [38,43].

Another example was the observation of selected SNO modifications on 7 of 34 Cys residues in protein FHL1 (four and a half LIM domains protein 1). The LIM domain binds zinc ions and mediates protein–protein interactions that are critical to cellular processes. FHL1, expressed in skeletal and cardiac muscle,

Table 1
Selected SNO-sensitive Cys-peptides from ALBU (serum albumin), AT2A1 (sarcoplasmic/endoplasmic reticulum calcium ATPase 1), FHL1 (four and a half LIM domains protein 1), and G3P (glyceraldehyde-3-phosphate dehydrogenase) proteins.

Peptide	Reference	Cys site	Avg $R_{10/100}$	$R_{10/100}$_a	$R_{10/100}$_b	SD $R_{10/100}$
K.GLVLIAFSQYLQKCSYDEHAK.L	ALBU_mouse	58	0.68	—[a]	0.68	—
R.YNDLGEQHFKGLVLIAFSQYLQKCSYDEHAK.L	ALBU_mouse	58	0.64	—	0.64	—
K.STEECLSYFGVSETTGLTPDQVK.R	AT2A1_mouse	12	0.28	0.20	0.36	0.12
K.STEECLSYFGVSETTGLTPDQVKR.H	AT2A1_mouse	12	0.23	0.14	0.31	0.12
R.SLPSVETLGCTSVIC#SDK.T	AT2A1_mouse	344	0.43	0.34	0.53	0.13
R.SLPSVETLGC#TSVICSDK.T	AT2A1_mouse	349	0.45	0.36	0.53	0.12
R.SLPSVETLGCTSVICSDK.T	AT2A1_mouse	344, 349	0.32	0.25	0.39	0.10
R.SLPSVETLGCTSVICSDKTGTLTTNQMSVC#K.M	AT2A1_mouse	344, 349	0.32	0.32	0.32	0.00
K.TGTLTTNQMSVCK.M	AT2A1_mouse	364	0.20	0.15	0.25	0.08
K.MFIIDKVDGDVCSLNEFSITGSTYAPEGEVLK.N	AT2A1_mouse	377	0.22	0.16	0.28	0.09
R.AGQYDGLVELATICALC#NDSSLDFNETK.G	AT2A1_mouse	417	0.24	0.11	0.38	0.20
R.AGQYDGLVELATIC#ALCNDSSLDFNETK.G	AT2A1_mouse	420	0.27	0.33	0.21	0.09
R.ANACNSVIR.Q	AT2A1_mouse	471	0.39	0.31	0.47	0.11
K.SMSVYCSPAK.S	AT2A1_mouse	498	0.29	0.23	0.36	0.09
R.KSMSVYCSPAK.S	AT2A1_mouse	498	0.34	0.30	0.37	0.05
K.GAPEGVIDRCNYVR.V	AT2A1_mouse	525	0.37	0.37	0.36	0.01
R.CLALATR.D	AT2A1_mouse	561	0.23	0.23	—	—
K.EVTGSIQLCR.D	AT2A1_mouse	614	0.40	0.29	0.51	0.16
K.GTAIAICR.R	AT2A1_mouse	636	0.72	—	0.72	—
R.EFDDLPLAEQREACRR.A	AT2A1_mouse	670	0.22	—	0.22	—
R.ACC#FAR.V	AT2A1_mouse	674	0.40	0.36	0.44	0.06
R.AC#CFAR.V	AT2A1_mouse	675	0.42	0.39	0.44	0.03
R.RACCFAR.V	AT2A1_mouse	674, 675	0.39	—	0.39	—
R.ACCFAR.V	AT2A1_mouse	674, 675	0.33	0.27	0.38	0.08
K.FDCHYC#R.D	FHL1_mouse	7	0.24	0.24	—	—
K.FDC#HYCRDPLQGK.K	FHL1_mouse	10	0.21	0.21	—	—
K.FDCHYCRDPLQGK.K	FHL1_mouse	7, 10	0.21	0.16	0.25	0.06
K.GEDFYCVTCHETK.F	FHL1_mouse	150, 153	0.26	0.19	0.33	0.10
K.QVIGTGSFFPKGEDFYCVTCHETK.F	FHL1_mouse	150, 153	0.37	0.33	0.41	0.05
R.FTAVEDQYYCVDCYKNFVAK.K	FHL1_mouse	209, 212	0.25	0.26	0.23	0.02
K.GSSVVAYEGQSWHDYCFHC#K.K	FHL1_mouse	249	0.47	0.67	0.27	0.28
R.AAICSGK.V	G3P_mouse	22	0.59	0.49	0.69	0.14
K.IVSNASC#TTNCLAPLAK.V	G3P_mouse	154	0.44	0.46	0.42	0.03
R.VPTPNVSVVDLTCRLEKPAK.Y	G3P_mouse	245	0.46	0.50	0.42	0.06
K.IVSNASCTTNCLAPLAK.V	G3P_mouse	150, 154	0.29	0.31	0.28	0.02

Average and standard deviation (SD) values of $R_{10/100}$ were calculated from two independent experiments. "#" designates NEM modification, not an SNO-modified Cys site.

[a] Either not detected or not quantifiable because the reporter ion intensity from the 10 μM treatment is below the detection limit.

is localized in both the cytoplasm and the nucleus [73]. The observed SNO-sensitive sites C7, C10, C150, C153, C209, C212, and C249 were located in zinc-binding domain 2 (101–153), domain 3 (162–212), domain 4 (212–276), and zinc-finger (7–10), where the binding to Zn^{2+} might lead to a lower pK_a of the thiols, thus making it more nucleophilic. It is possible that S-nitrosylation on these cysteines plays a role in regulating the interaction between FHL1 and its target proteins, although the exact biological role of S-nitrosylation of FHL1 is yet to be established.

Sarcoplasmic/endoplasmic reticulum calcium ATPase 1 (SERCA1 or AT2A1) was another example of a cysteine-rich protein that contains 24 cysteine residues with one disulfide formed between C876 and C888. It catalyzes the hydrolysis of ATP coupled with the translocation of calcium from the cytosol to the sarcoplasmic reticulum lumen, constituting the rate-limiting step of muscle relaxation. Among the free cysteines, we identified 15 of 22 (C12, C344, C349, C364, C377, C417, C471, C498, C525, C561, C614, C636, C670, C674, and C675) as SNO-sensitive sites. Our results were in good agreement with the previous reports [74,75] in which all these sites were also observed to be SNO sensitive, indicating that protein AT2A1 is very susceptible to S-nitrosylation on many Cys sites. In particular, C344, C349, and C364 are in the vicinity of the catalytic phosphoenzyme site, D351, suggesting that S-nitrosylation may regulate enzyme activity. Moreover, SERCA1 was also reported to bind to insulin receptor substrate proteins in an insulin-regulated fashion [76], and SNO on SERCA1 can potentially play a role in insulin action.

Functional analysis of S-nitrosylation-sensitive proteins

To further examine the functional categories of these SNO-sensitive proteins, functional analyses were performed based on gene ontology annotations and KEGG pathways. As shown in Fig. 6A, the majority of these proteins originated from mitochondria (34%), contractile fiber (13%), cytoskeleton (12%), and cytosol (10%), suggesting the potential significance of SNO-mediated regulation in these cellular components. Fig. 6B illustrates the top KEGG pathways that involve the SNO-sensitive proteins. A number of metabolic pathways, including the tricarboxylic acid (TCA) cycle, glycolysis/gluconeogenesis, glutathione metabolism, oxidative phosphorylation, and fatty acid metabolism, were observed with high significance, which was consistent with the observation of many SNO modifications in mitochondria, because all of these metabolic pathways involve many mitochondrial enzymes. Identified SNO-sensitive enzymes involved in the TCA cycle include citrate synthase, aconitase, isocitrate dehydrogenase 1 and 2, succinyl-CoA ligase, succinate dehydrogenase, and malate dehydrogenase. A number of key glycolysis enzymes were also identified as SNO-sensitive proteins, including hexokinase, glucose phosphate isomerase, phosphofructokinase, fructose biphosphatase, phosphoglycerate mutase, and enolase. Several proteins involved in glutathione metabolism such as glutathione *S*-transferases Kappa 1, Mu 1, and Mu 5 were also observed as SNO-sensitive proteins. The observation of a variety of metabolic enzymes identified as SNO-sensitive proteins suggested that S-nitrosylation

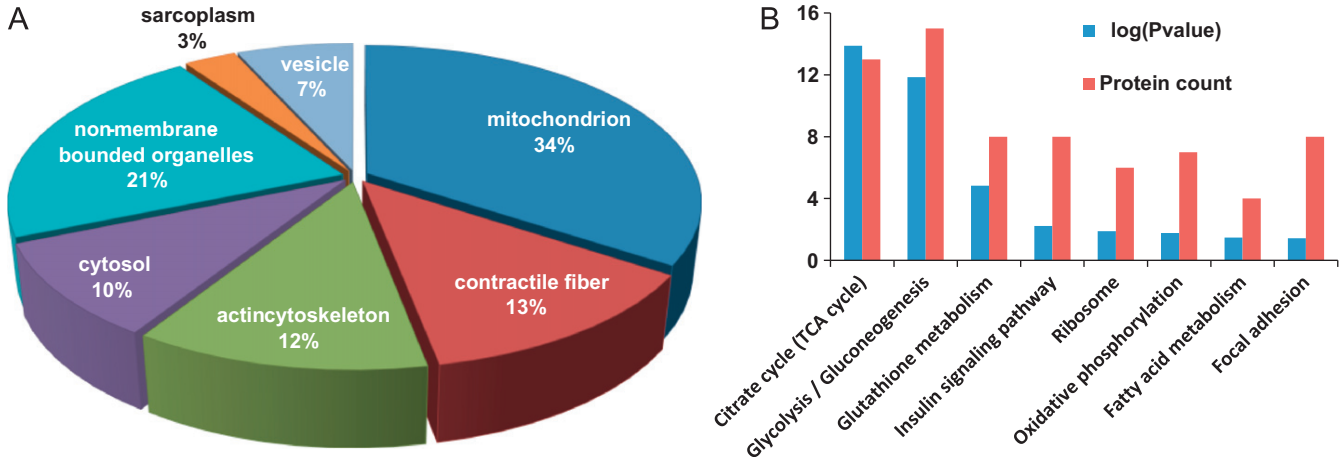

Fig. 6. (A) Subcellular components and (B) top KEGG pathways of the identified SNO-sensitive proteins.

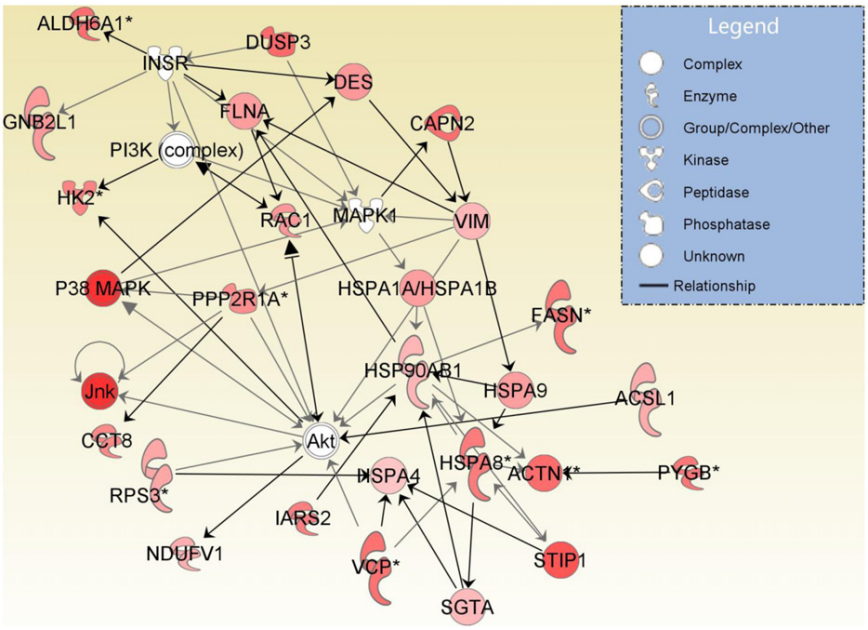

Fig. 7. A protein interaction network representative of SNO-sensitive proteins. The color intensity correlates with the number of identified SNO sites.

is an important redox-based mechanism for regulating metabolic enzyme activities. This observation was in good agreement with literature reports that many key metabolic enzymes in eukaryotic cells contain redox-sensitive active-site cysteine residues [77,78].

In addition to the role in regulating metabolic enzyme activities, S-nitrosylation plays an important role in signal transduction. An example is the insulin-signaling pathway, which is critical for the regulation of glucose uptake, glycolysis, and fatty acid metabolism. The potential significance of S-nitrosylation in mediating insulin signaling in mouse muscle has been reported in key insulin-signaling proteins such as insulin receptor, insulin receptor substrate proteins, and Akt [79]. Although the direct SNO modifications on these known proteins were not observed in this study, presumably because of insufficient sensitivity to detect low-abundance proteins, a number of other proteins associated with the insulin-signaling pathway were identified as sensitive to S-nitrosylation. These SNO-sensitive proteins included phosphorylase kinases α1, β, and γ1, a family of serine/threonine-specific protein kinases that activate glycogen phosphorylase to release glucose 1-phosphate from glycogen.

The datasets also contained a number of other SNO-sensitive proteins that may play a role in cell signaling. Fig. 7 shows a protein interaction network that contained many SNO-sensitive signaling proteins. Interestingly, SNO modifications were observed on a number of serine/threonine kinases (e.g., MAPK1, p38 MAPK), phosphatases (e.g., DUSP3, PPP2R1A), and stress-response proteins (e.g., JNK, heat shock proteins), which may directly or indirectly interact with other signaling pathways such as insulin signaling. For example, p38 MAPK is known to play a key role in stress-induced IRS-1 serine phosphorylation and insulin resistance [80]. The observed SNO modification on p38 MAPK can be a possible mechanism for modulating its activity in response to oxidative stress. The potential role of reversible modifications on p38 MAPK and other signaling proteins should warrant detailed investigation.

Conclusions

Our results demonstrate the sensitivity and specificity of an optimized resin-assisted cysteinyl peptide enrichment approach for site-specific detection and quantification of S-nitrosylation in complex proteome samples at both peptide- and protein-level enrichments. The application to quantitative reactivity profiling of S-nitrosylation in mouse muscle led to identification of 488 SNO sites from 197 proteins with different levels of sensitivity to S-nitrosylation. Many of the observed SNO proteins are localized in mitochondria, contractile fiber, and actin cytoskeleton, suggesting the susceptibility of these subcellular compartments to redox regulation. Many of the SNO-sensitive proteins are metabolic enzymes associated with the TCA cycle, glycolysis/gluconeogenesis, glutathione metabolism, and fatty acid metabolism, highlighting the importance of redox regulation in metabolism. Moreover, a number of signaling proteins were also identified as being SNO sensitive, suggesting the role of S-nitrosylation in signaling transduction. Discovery of the SNO-sensitive cysteine residues in a particular cell or tissue type would provide valuable information for understanding the nature of S-nitrosylation in cellular signaling pathways and in pathophysiology such as insulin resistance and diabetes.

Acknowledgments

Portions of this work were supported by the NIH Director's New Innovator Award Program DP2OD006668, a DOE Early Career Research Award, and NIH Grants R01 DK074795, P41 RR018522, and P41 GM103493. Experimental work was performed in the Environmental Molecular Science Laboratory, a DOE/BER national scientific user facility at PNNL in Richland, Washington. PNNL is operated by Battelle for the DOE under Contract DE-AC05-76RLO-1830.

Appendix A. Supporting information

Supplementary data associated with this article can be found in the online version at http://dx.doi.org/10.1016/j.freeradbiomed.2012.12.010.

References

[1] Stamler, J. S.; Hausladen, A. Oxidative modifications in nitrosative stress. *Nat. Struct. Biol* **5:**247–249; 1998.
[2] Filomeni, G.; Rotilio, G.; Ciriolo, M. R. Disulfide relays and phosphorylative cascades: partners in redox-mediated signaling pathways. *Cell Death Differ.* **12:**1555–1563; 2005.
[3] Eaton, P. Protein thiol oxidation in health and disease: techniques for measuring disulfides and related modifications in complex protein mixtures. *Free Radic. Biol. Med* **40:**1889–1899; 2006.
[4] Riederer, B. M. Oxidation proteomics: the role of thiol modifications. *Curr. Proteomics* **6:**51–62; 2009.
[5] Janssen-Heininger, Y. M.; Mossman, B. T.; Heintz, N. H.; Forman, H. J.; Kalyanaraman, B.; Finkel, T.; Stamler, J. S.; Rhee, S. G.; van der Vliet, A. Redox-based regulation of signal transduction: principles, pitfalls, and promises. *Free Radic. Biol. Med.* **45:**1–17; 2008.
[6] Paulsen, C. E.; Carroll, K. S. Orchestrating redox signaling networks through regulatory cysteine switches. *ACS Chem. Biol.* **5:**47–62; 2010.
[7] Stamler, J. S. Redox signaling: nitrosylation and related target interactions of nitric oxide. *Cell* **78:**931–936; 1994.
[8] Gaston, B. Nitric oxide and thiol groups. *Biochim. Biophys. Acta* **1411:**323–333; 1999.
[9] Lane, P.; Hao, G.; Gross, S. S. S-nitrosylation is emerging as a specific and fundamental posttranslational protein modification: head-to-head comparison with O-phosphorylation. *Sci. STKE 2001:re1* ; 2001.
[10] Martinez-Ruiz, A.; Lamas, S. S-nitrosylation: a potential new paradigm in signal transduction. *Cardiovasc. Res.* **62:**43–52; 2004.
[11] Hess, D. T.; Matsumoto, A.; Kim, S. O.; Marshall, H. E.; Stamler, J. S. Protein S-nitrosylation: purview and parameters. *Nat. Rev. Mol. Cell. Biol.* **6:**150–166; 2005.
[12] Wang, Y.; Yun, B. W.; Kwon, E.; Hong, J. K.; Yoon, J.; Loake, G. J. S-nitrosylation: an emerging redox-based post-translational modification in plants. *J. Exp. Bot.* **57:**1777–1784; 2006.
[13] Duan, S.; Chen, C. S-nitrosylation/denitrosylation and apoptosis of immune cells. *Cell. Mol. Immunol.* **4:**353–358; 2007.
[14] Abat, J. K.; Saigal, P.; Deswal, R. S-Nitrosylation—another biological switch like phosphorylation? *Physiol. Mol. Biol. Plants* **14:**119–130; 2008.
[15] Stamler, J. S.; Sun, Q. A.; Hess, D. T. A SNO storm in skeletal muscle. *Cell* **133:**33–35; 2008.
[16] Dalle-Donne, I.; Rossi, R.; Colombo, G.; Giustarini, D.; Milzani, A. Protein S-glutathionylation: a regulatory device from bacteria to humans. *Trends Biochem. Sci.* **34:**85–96; 2009.
[17] Foster, M. W.; Hess, D. T.; Stamler, J. S. Protein S-nitrosylation in health and disease: a current perspective. *Trends Mol. Med.* **15:**391–404; 2009.
[18] Lima, B.; Forrester, M. T.; Hess, D. T.; Stamler, J. S. S-nitrosylation in cardiovascular signaling. *Circ. Res.* **106:**633–646; 2010.
[19] Sun, J.; Murphy, E. Protein S-nitrosylation and cardioprotection. *Circ. Res.* **106:**285–296; 2010.
[20] Nakamura, T.; Lipton, S. A. Redox modulation by S-nitrosylation contributes to protein misfolding, mitochondrial dynamics, and neuronal synaptic damage in neurodegenerative diseases. *Cell Death Differ* **18:**1478–1486; 2011.
[21] Seth, D.; Stamler, J. S. The SNO-proteome: causation and classifications. *Curr. Opin. Chem. Biol.* **15:**129–136; 2011.
[22] Benhar, M.; Stamler, J. S. A central role for S-nitrosylation in apoptosis. *Nat. Cell Biol.* **7:**645–646; 2005.
[23] Beigi, F.; Gonzalez, D. R.; Minhas, K. M.; Sun, Q. A.; Foster, M. W.; Khan, S. A.; Treuer, A. V.; Dulce, R. A.; Harrison, R. W.; Saraiva, R. M.; Premer, C.; Schulman, I. H.; Stamler, J. S.; Hare, J. M. Dynamic denitrosylation via S-nitrosoglutathione reductase regulates cardiovascular function. *Proc. Natl. Acad. Sci. USA* **109:**4314–4319; 2012.
[24] Benhar, M.; Forrester, M. T.; Stamler, J. S. Protein denitrosylation: enzymatic mechanisms and cellular functions. *Nature Rev. Mol. Cell Biol.* **10:**721–732; 2009.
[25] Benhar, M.; Forrester, M. T.; Hess, D. T.; Stamler, J. S. Regulated protein denitrosylation by cytosolic and mitochondrial thioredoxins. *Science* **320:**1050–1054; 2008.
[26] Weerapana, E.; Wang, C.; Simon, G. M.; Richter, F.; Khare, S.; Dillon, M. B.; Bachovchin, D. A.; Mowen, K.; Baker, D.; Cravatt, B. F. Quantitative reactivity profiling predicts functional cysteines in proteomes. *Nature* **468:**790–795; 2010.
[27] Powers, S. K.; Talbert, E. E.; Adhihetty, P. J. Reactive oxygen and nitrogen species as intracellular signals in skeletal muscle. *J. Physiol.* **589:**2129–2138; 2011.
[28] Jackson, M. J.; McArdle, A. Age-related changes in skeletal muscle reactive oxygen species generation and adaptive responses to reactive oxygen species. *J. Physiol* **589:**2139–2145; 2011.
[29] Carvalho-Filho, M. A.; Ropelle, E. R.; Pauli, R. J.; Cintra, D. E.; Tsukumo, D. M.; Silveira, L. R.; Curi, R.; Carvalheira, J. B.; Velloso, L. A.; Saad, M. J. Aspirin attenuates insulin resistance in muscle of diet-induced obese rats by inhibiting inducible nitric oxide synthase production and S-nitrosylation of IRbeta/IRS-1 and Akt. *Diabetologia* **52:**2425–2434; 2009.
[30] Bellinger, A. M.; Reiken, S.; Carlson, C.; Mongillo, M.; Liu, X.; Rothman, L.; Matecki, S.; Lacampagne, A.; Marks, A. R. Hypernitrosylated ryanodine receptor calcium release channels are leaky in dystrophic muscle. *Nat. Med* **15:**325–330; 2009.
[31] Xu, L.; Eu, J. P.; Meissner, G.; Stamler, J. S. Activation of the cardiac calcium release channel (ryanodine receptor) by poly-S-nitrosylation. *Science* **279:**234–237; 1998.
[32] Greco, T. M.; Hodara, R.; Parastatidis, I.; Heijnen, H. F.; Dennehy, M. K.; Liebler, D. C.; Ischiropoulos, H. Identification of S-nitrosylation motifs by site-specific mapping of the S-nitrosocysteine proteome in human vascular smooth muscle cells. *Proc. Natl. Acad. Sci. USA* **103:**7420–7425; 2006.
[33] Kohr, M. J.; Aponte, A. M.; Sun, J.; Wang, G.; Murphy, E.; Gucek, M.; Steenbergen, C. Characterization of potential S-nitrosylation sites in the myocardium. *Am. J. Physiol. Heart Circ. Physiol* **300:**H1327–1335; 2011.
[34] Raju, K.; Doulias, P. T.; Tenopoulou, M.; Greene, J. L.; Ischiropoulos, H. Strategies and tools to explore protein S-nitrosylation. *Biochim. Biophys. Acta* **1820:**684–688; 2012.
[35] Jaffrey, S. R.; Erdjument-Bromage, H.; Ferris, C. D.; Tempst, P.; Snyder, S. H. Protein S-nitrosylation: a physiological signal for neuronal nitric oxide. *Nat. Cell Biol.* **3:**193–197; 2001.
[36] Jaffrey, S. R.; Snyder, S. H. The biotin switch method for the detection of S-nitrosylated proteins. *Sci. STKE 2001:pl1* ; 2001.
[37] Forrester, M. T.; Foster, M. W.; Benhar, M.; Stamler, J. S. Detection of protein S-nitrosylation with the biotin-switch technique. *Free Radic. Biol. Med.* **46:**119–126; 2009.
[38] Hao, G.; Derakhshan, B.; Shi, L.; Campagne, F.; Gross, S. S. SNOSID, a proteomic method for identification of cysteine S-nitrosylation sites in complex protein mixtures. *Proc. Natl. Acad. Sci. USA* **103:**1012–1017; 2006.
[39] Huang, B.; Chen, C. Detection of protein S-nitrosation using irreversible biotinylation procedures (IBP). *Free Radic. Biol. Med.* **49:**447–456; 2010.
[40] Wu, C.; Parrott, A. M.; Liu, T.; Jain, M. R.; Yang, Y.; Sadoshima, J.; Li, H. Distinction of thioredoxin transnitrosylation and denitrosylation target proteins by the ICAT quantitative approach. *J. Proteomics* **74:**2498–2509; 2011.

[41] Murray, C. I.; Uhrigshardt, H.; O'Meally, R. N.; Cole, R. N.; Van Eyk, J. E. Identification and quantification of S-nitrosylation by cysteine reactive tandem mass tag switch assay. *Mol. Cell. Proteomics* **11(M111):**013441; 2012.
[42] Forrester, M. T.; Thompson, J. W.; Foster, M. W.; Nogueira, L.; Moseley, M. A.; Stamler, J. S. Proteomic analysis of S-nitrosylation and denitrosylation by resin-assisted capture. *Nat. Biotechnol.* **27:**557–559; 2009.
[43] Liu, M.; Hou, J.; Huang, L.; Huang, X.; Heibeck, T. H.; Zhao, R.; Pasa-Tolic, L.; Smith, R. D.; Li, Y.; Fu, K.; Zhang, Z.; Hinrichs, S. H.; Ding, S. J. Site-specific proteomics approach for study protein S-nitrosylation. *Anal. Chem.* **82:**7160–7168; 2010.
[44] Liu, T.; Qian, W. J.; Strittmatter, E. F.; Camp, D. G.; Anderson, G. A.; Thrall, B. D.; Smith, R. D. High throughput comparative proteome analysis using a quantitative cysteinyl-peptide enrichment technology. *Anal. Chem.* **76:**5345–5353; 2004.
[45] Gaston, B.; Reilly, J.; Drazen, J. M.; Fackler, J.; Ramdev, P.; Arnelle, D.; Mullins, M. E.; Sugarbaker, D. J.; Chee, C.; Singel, D. J., et al. Endogenous nitrogen oxides and bronchodilator S-nitrosothiols in human airways. *Proc. Natl. Acad. Sci. USA* **90:**10957–10961; 1993.
[46] Kluge, I.; Gutteck-Amsler, U.; Zollinger, M.; Do, K. Q. S-nitrosoglutathione in rat cerebellum: identification and quantification by liquid chromatography–mass spectrometry. *J. Neurochem.* **69:**2599–2607; 1997.
[47] Wisniewski, J. R.; Zougman, A.; Nagaraj, N.; Mann, M. Universal sample preparation method for proteome analysis. *Nat. Methods* **6:**359–362; 2009.
[48] Liu, T.; Qian, W. J.; Strittmatter, E. F.; Camp 2nd D. G.; Anderson, G. A.; Thrall, B. D.; Smith, R. D. High-throughput comparative proteome analysis using a quantitative cysteinyl-peptide enrichment technology. *Anal. Chem.* **76:**5345–5353; 2004.
[49] Liu, T.; Qian, W. J.; Chen, W. N.; Jacobs, J. M.; Moore, R. J.; Anderson, D. J.; Gritsenko, M. A.; Monroe, M. E.; Thrall, B. D.; Camp 2nd D. G.; Smith, R. D. Improved proteome coverage by using high efficiency cysteinyl peptide enrichment: the human mammary epithelial cell proteome. *Proteomics* **5:**1263–1273; 2005.
[50] Mannick, J. B.; Schonhoff, C. M. Analysis of protein S-nitrosylation. *Curr. Protoc. Protein Sci. Chap.* **14(Unit 14):**16; 2006.
[51] Livesay, E. A.; Tang, K.; Taylor, B. K.; Buschbach, M. A.; Hopkins, D. F.; LaMarche, B. L.; Zhao, R.; Shen, Y.; Orton, D. J.; Moore, R. J.; Kelly, R. T.; Udseth, H. R.; Smith, R. D. Fully automated four-column capillary LC–MS system for maximizing throughput in proteomic analyses. *Anal. Chem.* **80:**294–302; 2008.
[52] Kelly, R. T.; Page, J. S.; Luo, Q.; Moore, R. J.; Orton, D. J.; Tang, K.; Smith, R. D. Chemically etched open tubular and monolithic emitters for nanoelectrospray ionization mass spectrometry. *Anal. Chem.* **78:**7796–7801; 2006.
[53] Eng, J. K.; McCormack, A. L.; Yates, J. R. An approach to correlate tandem mass spectral data of peptides with amino acid sequences in a protein database. *J. Am. Soc. Mass Spectrom* **5:**976–989; 1994.
[54] Elias, J. E.; Gygi, S. P. Target-decoy search strategy for increased confidence in large-scale protein identifications by mass spectrometry. *Nat. Methods* **4:**207–214; 2007.
[55] Qian, W. J.; Liu, T.; Monroe, M. E.; Strittmatter, E. F.; Jacobs, J. M.; Kangas, L. J.; Petritis, K.; Camp, D. G.; Smith, R. D. Probability-based evaluation of peptide and protein identifications from tandem mass spectrometry and SEQUEST analysis: the human proteome. *J. Proteome Res.* **4:**53–62; 2005.
[56] Kim, S.; Gupta, N.; Pevzner, P. A. Spectral probabilities and generating functions of tandem mass spectra: a strike against decoy databases. *J. Proteome Res.* **7:**3354–3363; 2008.
[57] Huang da, W.; Sherman, B. T.; Lempicki, R. A. Systematic and integrative analysis of large gene lists using DAVID bioinformatics resources. *Nat. Protoc.* **4:**44–57; 2009.
[58] Huang da, W.; Sherman, B. T.; Lempicki, R. A. Bioinformatics enrichment tools: paths toward the comprehensive functional analysis of large gene lists. *Nucleic Acids Res.* **37:**1–13; 2009.
[59] Zhang, Y.; Keszler, A.; Broniowska, K. A.; Hogg, N. Characterization and application of the biotin-switch assay for the identification of S-nitrosated proteins. *Free Radic. Biol. Med.* **38:**874–881; 2005.
[60] Huang, B.; Chen, C. An ascorbate-dependent artifact that interferes with the interpretation of the biotin switch assay. *Free Radic. Biol. Med* **41:**562–567; 2006.
[61] Forrester, M. T.; Foster, M. W.; Stamler, J. S. Assessment and application of the biotin switch technique for examining protein S-nitrosylation under conditions of pharmacologically induced oxidative stress. *J. Biol. Chem* **282:**13977–13983; 2007.
[62] Kettenhofen, N. J.; Broniowska, K. A.; Keszler, A.; Zhang, Y.; Hogg, N. Proteomic methods for analysis of S-nitrosation. *J. Chromatogr. B. Anal. Technol. Biomed. Life Sci.* **851:**152–159; 2007.
[63] Giustarini, D.; Dalle-Donne, I.; Colombo, R.; Milzani, A.; Rossi, R. Is ascorbate able to reduce disulfide bridges? A cautionary note *Nitric Oxide* **19:**252–258; 2008.
[64] Wang, X.; Kettenhofen, N. J.; Shiva, S.; Hogg, N.; Gladwin, M. T. Copper dependence of the biotin switch assay: modified assay for measuring cellular and blood nitrosated proteins. *Free Radic. Biol. Med.* **44:**1362–1372; 2008.
[65] Kallakunta, V. M.; Staruch, A.; Mutus, B. Sinapinic acid can replace ascorbate in the biotin switch assay. *Biochim. Biophys. Acta* **1800:**23–30; 2010.
[66] Ross, P. L.; Huang, Y. N.; Marchese, J. N.; Williamson, B.; Parker, K.; Hattan, S.; Khainovski, N.; Pillai, S.; Dey, S.; Daniels, S.; Purkayastha, S.; Juhasz, P.; Martin, S.; Bartlet-Jones, M.; He, F.; Jacobson, A.; Pappin, D. J. Multiplexed protein quantitation in Saccharomyces cerevisiae using amine-reactive isobaric tagging reagents. *Mol. Cell. Proteomics* **3:**1154–1169; 2004.
[67] Choe, L.; D'Ascenzo, M.; Relkin, N. R.; Pappin, D.; Ross, P.; Williamson, B.; Guertin, S.; Pribil, P.; Lee, K. H. 8-plex quantitation of changes in cerebrospinal fluid protein expression in subjects undergoing intravenous immunoglobulin treatment for Alzheimer's disease. *Proteomics* **7:**3651–3660; 2007.
[68] Bulaj, G.; Kortemme, T.; Goldenberg, D. P. Ionization-reactivity relationships for cysteine thiols in polypeptides. *Biochemistry* **37:**8965–8972; 1998.
[69] Mohr, S.; Stamler, J. S.; Brune, B. Posttranslational modification of glyceraldehyde-3-phosphate dehydrogenase by S-nitrosylation and subsequent NADH attachment. *J. Biol. Chem.* **271:**4209–4214; 1996.
[70] Hara, M. R.; Agrawal, N.; Kim, S. F.; Cascio, M. B.; Fujimuro, M.; Ozeki, Y.; Takahashi, M.; Cheah, J. H.; Tankou, S. K.; Hester, L. D.; Ferris, C. D.; Hayward, S. D.; Snyder, S. H.; Sawa, A. S-nitrosylated GAPDH initiates apoptotic cell death by nuclear translocation following Siah1 binding. *Nat. Cell Biol.* **7:**665–674; 2005.
[71] Mustafa, A. K.; Gadalla, M. M.; Sen, N.; Kim, S.; Mu, W.; Gazi, S. K.; Barrow, R. K.; Yang, G.; Wang, R.; Snyder, S. H. H2S signals through protein S-sulfhydration. *Sci. Signaling* **2(ra72)**; 2009.
[72] Nemeth-Cawley, J. F.; Tangarone, B. S.; Rouse, J. C. Top down characterization is a complementary technique to peptide sequencing for identifying protein species in complex mixtures. *J. Proteome Res* **2:**495–505; 2003.
[73] Lee, S. M.; Tsui, S. K.; Chan, K. K.; Garcia-Barcelo, M.; Waye, M. M.; Fung, K. P.; Liew, C. C.; Lee, C. Y. Chromosomal mapping, tissue distribution and cDNA sequence of four-and-a-half LIM domain protein 1 (FHL1). *Gene* **216:**163–170; 1998.
[74] Viner, R. I.; Williams, T. D.; Schoneich, C. Peroxynitrite modification of protein thiols: oxidation, nitrosylation, and S-glutathiolation of functionally important cysteine residue(s) in the sarcoplasmic reticulum Ca-ATPase. *Biochemistry* **38:**12408–12415; 1999.
[75] Viner, R. I.; Williams, T. D.; Schoneich, C. Nitric oxide-dependent modification of the sarcoplasmic reticulum Ca-ATPase: localization of cysteine target sites. *Free Radic. Biol. Med.* **29:**489–496; 2000.
[76] Algenstaedt, P.; Antonetti, D. A.; Yaffe, M. B.; Kahn, C. R. Insulin receptor substrate proteins create a link between the tyrosine phosphorylation cascade and the Ca2+-ATPases in muscle and heart. *J. Biol. Chem.* **272:**23696–23702; 1997.
[77] Ziegler, D. M. Role of reversible oxidation–reduction of enzyme thiols–disulfides in metabolic regulation. *Annu. Rev. Biochem* **54:**305–329; 1985.
[78] Brandes, N.; Schmitt, S.; Jakob, U. Thiol-based redox switches in eukaryotic proteins. *Antioxid. Redox Signaling* **11:**997–1014; 2009.
[79] Carvalho-Filho, M. A.; Ueno, M.; Hirabara, S. M.; Seabra, A. B.; Carvalheira, J. B.; de Oliveira, M. G.; Velloso, L. A.; Curi, R.; Saad, M. J. S-nitrosation of the insulin receptor, insulin receptor substrate 1, and protein kinase B/Akt: a novel mechanism of insulin resistance. *Diabetes* **54:**959–967; 2005.
[80] Hemi, R.; Yochananov, Y.; Barhod, E.; Kasher-Meron, M.; Karasik, A.; Tirosh, A.; Kanety, H. p38 mitogen-activated protein kinase-dependent transactivation of ErbB receptor family: a novel common mechanism for stress-induced IRS-1 serine phosphorylation and insulin resistance. *Diabetes* **60:**1134–1145; 2011.